JBC RESEARCH ARTICLE

Neurotoxic and cytotoxic peptides underlie the painful stings of the tree nettle *Urtica ferox*

Received for publication, January 26, 2022, and in revised form, June 22, 2022 Published, Papers in Press, June 30, 2022,
https://doi.org/10.1016/j.jbc.2022.102218

Jing Xie[1,‡], Samuel D. Robinson[1,‡], Edward K. Gilding[1,‡], Sina Jami[1], Jennifer R. Deuis[1], Fabian B. H. Rehm[1], Kuok Yap[1], Lotten Ragnarsson[1], Lai Yue Chan[1], Brett R. Hamilton[2], Peta J. Harvey[1], David J. Craik[1,3], Irina Vetter[1,4,*], and Thomas Durek[1,3,*]

From the [1]Institute for Molecular Bioscience, [2]Centre for Microscopy and Microanalysis, [3]Australian Research Council Centre of Excellence for Innovations in Peptide and Protein Science, and [4]School of Pharmacy, The University of Queensland, Brisbane, Queensland, Australia

Edited by Mike Shipston

The stinging hairs of plants from the family Urticaceae inject compounds that inflict pain to deter herbivores. The sting of the New Zealand tree nettle (*Urtica ferox*) is among the most painful of these and can cause systemic symptoms that can even be life-threatening; however, the molecular species effecting this response have not been elucidated. Here we reveal that two classes of peptide toxin are responsible for the symptoms of *U. ferox* stings: Δ-Uf1a is a cytotoxic thionin that causes pain *via* disruption of cell membranes, while β/δ-Uf2a defines a new class of neurotoxin that causes pain and systemic symptoms *via* modulation of voltage-gated sodium (Na_V) channels. We demonstrate using whole-cell patch-clamp electrophysiology experiments that β/δ-Uf2a is a potent modulator of human $Na_V1.5$ (EC_{50}: 55 nM), $Na_V1.6$ (EC_{50}: 0.86 nM), and $Na_V1.7$ (EC_{50}: 208 nM), where it shifts the activation threshold to more negative potentials and slows fast inactivation. We further found that both toxin classes are widespread among members of the *Urticeae* tribe within Urticaceae, suggesting that they are likely to be pain-causing agents underlying the stings of other *Urtica* species. Comparative analysis of nettles of *Urtica*, and the recently described pain-causing peptides from nettles of another genus, *Dendrocnide*, indicates that members of tribe *Urticeae* have developed a diverse arsenal of pain-causing peptides.

Plants produce a plethora of secondary metabolites for defense against microbes and herbivores (1, 2). These defense molecules are stored in various parts of the plant and are typically released upon tissue damage or ingestion of plant material, but some plants, most notably the "true stinging nettles" (family: Urticaceae, tribe: *Urticeae*), have specialized needle-like structures that deliver compounds intra- or subdermally. One such nettle is *Urtica ferox* (commonly known as ongaonga or the New Zealand tree nettle), which can grow up to 4 m high and is endemic to New Zealand. Its leaves and stems are covered with stinging hairs (trichomes) that can pierce skin and deliver venom (3, 4). Stings of *U. ferox* cause local skin irritation (contact urticaria), itching, and pain, as well as paresthesia and numbness. In severe cases, *U. ferox* stings can cause systemic effects, including neuromuscular and respiratory distress, ataxia and weakness, vision disturbances, and hypersalivation, which can last for days to weeks and have been well documented in dogs and humans (5–7). Anecdotal reports have implicated severe *U. ferox* stings in the deaths of humans and other vertebrates (8).

The toxin(s) responsible for these effects have not been identified. The trichomes of *U. ferox* are known to contain neurotransmitters such as acetylcholine, histamine, and serotonin (9), but it is generally accepted that these compounds alone cannot explain the complex and long-lasting pharmacological effects observed (10). Indeed, several studies have suggested the existence of uncharacterized neurotoxins in *U. ferox* trichomes (3, 6, 10–13).

Herein, we report the discovery and characterization of two classes of pain-causing peptides in trichome extracts of *U. ferox*, namely, Δ-Uf1a, a 4.3-kDa cytotoxic thionin, and β/δ-Uf2a, a 6.7-kDa peptide that is a potent activator of mammalian voltage-gated sodium channels. We show that orthologues of both toxin classes are found in other species of the tribe *Urticeae* (including the "common nettle" *Urtica dioica* and *Urtica incisa*), suggesting that these toxin classes may also be responsible for the painful effects experienced following envenomation by other stinging nettles.

Results

Identification of pain-causing compounds in U. ferox *trichomes*

U. ferox has characteristic white stinging trichomes up to 10 mm in length that are located predominantly on the stems, petioles, and the leaf midrib (Fig. 1*A*). We collected trichomes and extracted their contents in an acetonitrile/water mixture (50% (v/v)). Shallow intraplantar injection of the extract into the hind paw of mice (20 μl, 1 mg/ml) caused immediate and long-lasting pain-like behaviors including licking, shaking, and biting of the injected paw. To identify the pain-causing principles present in the extract, we fractionated it by

‡ These authors contributed equally to this work.
* For correspondence: Thomas Durek, t.durek@uq.edu.au; Irina Vetter, i.vetter@imb.uq.edu.au.

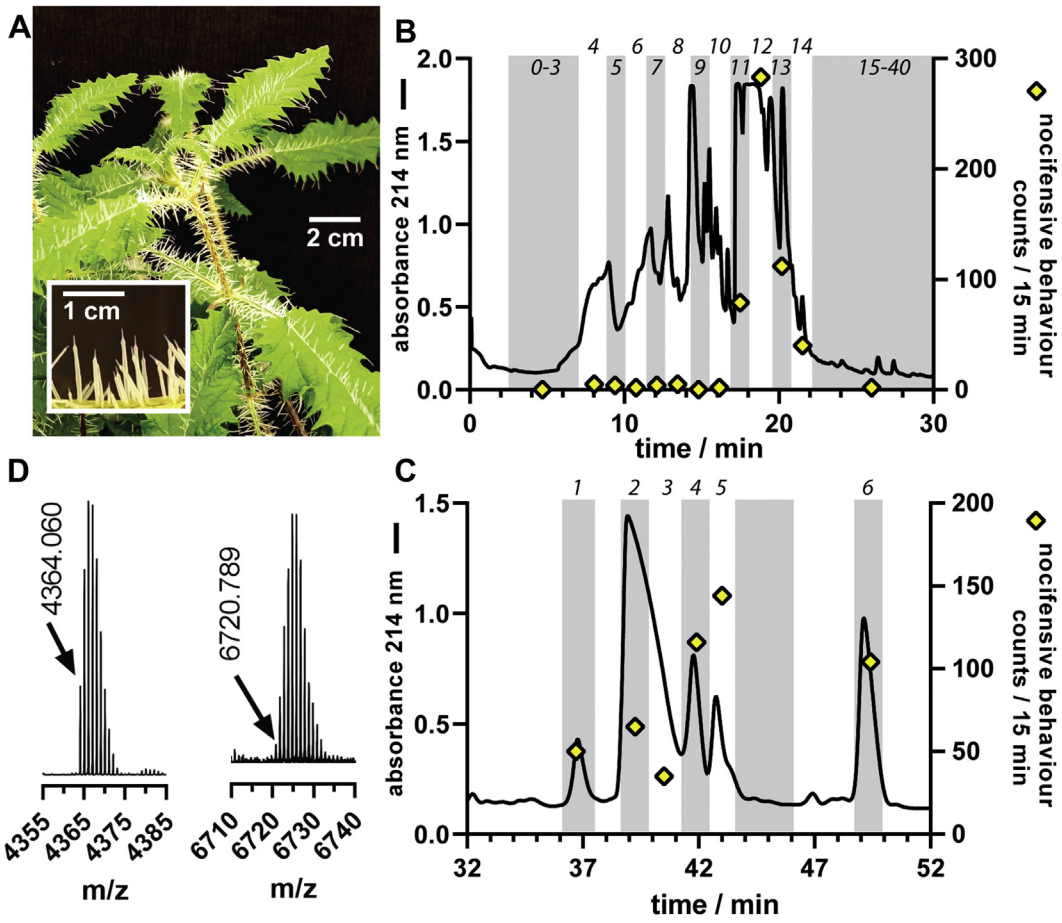

Figure 1. Pain-causing toxins in *Urtica ferox* trichome extracts. *A*, *U. ferox* is densely covered in white stinging hairs. The trichomes shown in the *inset* are approximately 8 mm long. *B*, fractionation of the crude stinging hair extract *via* RP-HPLC identified four sequentially eluting fractions (11–14) with pain-causing activity when injected intraplantar into mice (n = 1). *C*, further subfractionation of fraction 12 yielded six subfractions (12.1–12.6), which elicited varying degrees of nocifensive behaviors (n = 1). *D*, HR-MALDI-MS spectrum of the principal ions present in F12.2 (*left*) and F12.6 (*right*).

reversed-phase HPLC (RP-HPLC) and tested the capacity of each fraction to independently cause nocifensive responses in mice (Fig. 1*B*). Four sequentially eluting fractions caused spontaneous pain behaviors, with fraction 12 causing the strongest effect. HPLC/mass spectrometry (MS) analysis of fraction 12 indicated the presence of multiple components; we therefore performed an additional round of fractionation by RP-HPLC (Fig. 1*C*), which yielded six subfractions (12.1–12.6) that each caused some degree of nocifensive responses in mice following intraplantar injection. Subfractions 12.4 to 12.6 showed stronger activity than subfractions 12.1 to 12.3 (Fig. 1*C*), and we also noted qualitative differences between the two groups of three subfractions: Pain behaviors elicited by fractions 12.1 to 12.3 included a large proportion of licking/biting at the injected paw, which was noticeably swollen, while pain behaviors elicited by fractions 12.4 to 12.6 had a higher proportion of shaking and flinching of the injected paw.

We investigated the effects of the six subfractions on cultured mouse dorsal root ganglion (DRG) cells, which include nociceptive neurons. Consistent with the qualitative differences observed in our *in vivo* experiments, subfractions 12.4 to 12.6 caused an increase in $[Ca^{2+}]_i$ that was immediate, strong, sustained, and specific to neuronal cells (Fig. 2*A*). On the other hand, subfractions 12.1 to 12.3 caused an increase in $[Ca^{2+}]_i$ that was variable in onset, transient, and occurred in all cells (neuronal and nonneuronal) in the culture (Fig. 2*B*). The transient nature of this effect was due to leakage of the dye from the intracellular to extracellular space (Fig. 2*B*), an indication of compromised cell membranes. Together with our *in vivo* data, these results indicated that multiple pain-causing agents were present in our *U. ferox* trichome extracts and that these could be divided into two distinct mechanistic groups: a neuron-specific group, which we hereon refer to as neurotoxic (fractions 12.4–12.6), and a cytolytic group (fractions 12.1–12.3). Based on purity, we selected subfractions 12.2 (cytolytic) and 12.6 (neurotoxic) as representatives of the two mechanistic groups for further characterization.

High-resolution mass spectrometry on a timsTOF-fleX MALDI-2 system (Fig. 1*D*) coupled with tryptic digestion and tandem mass spectrometry (MSMS) analysis indicated that subfractions 12.2 and 12.6 were composed of peptides with molecular masses of 4364.060 Da and 6720.789 Da (monoisotopic $M + H^+$), respectively. Reduction and alkylation analysis indicated the presence of three disulfide bonds in the 4.3-kDa peptide and six disulfide bonds in the 6.7-kDa peptide. We determined the complete primary structure of both

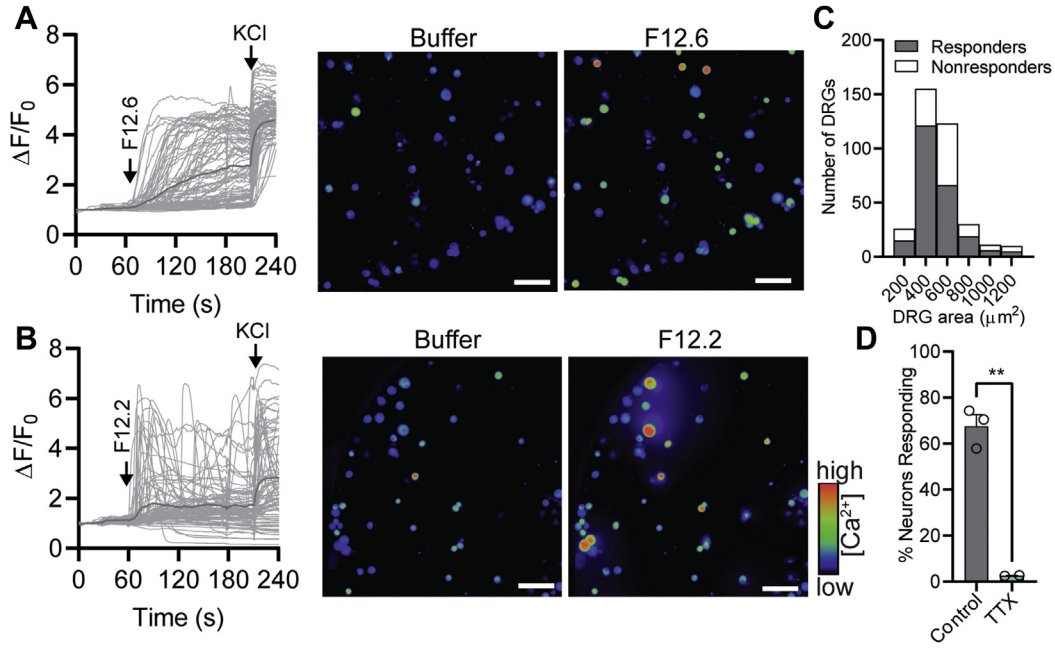

Figure 2. Activation of mouse DRG neurons by *U. ferox* pain-causing toxins. *A* and *B*, Ca^{2+} responses in mouse DRG cells of F12.2 (*A*) and F12.6 (*B*). Traces from all cells in a single representative experiment are shown in the *left panel*. The *dark gray trace* represents the average response. Pseudocolor images showing cells before (buffer) and after toxin application are shown to the *right* (The scale bar represents 100 μm). *C*, distribution of F12.6 responding and nonresponding cells by cell size. *D*, percentage of DRG neurons activated by F12.6 (440 nM) in the absence or presence of TTX (1 μM). Data are expressed as mean ± SEM.

molecules by analysis of MSMS fragmentation data (Fig. S1) and by searching a database of open reading frames predicted from mRNA sequencing of *U. ferox* leaves (Figs. 3*A* and 4*A*).

The cytolytic 4.3-kDa component (subfraction 12.2) is a 42-amino-acid peptide with high sequence identity (~80%) to viscotoxins and phoratoxins, which are families of thionin

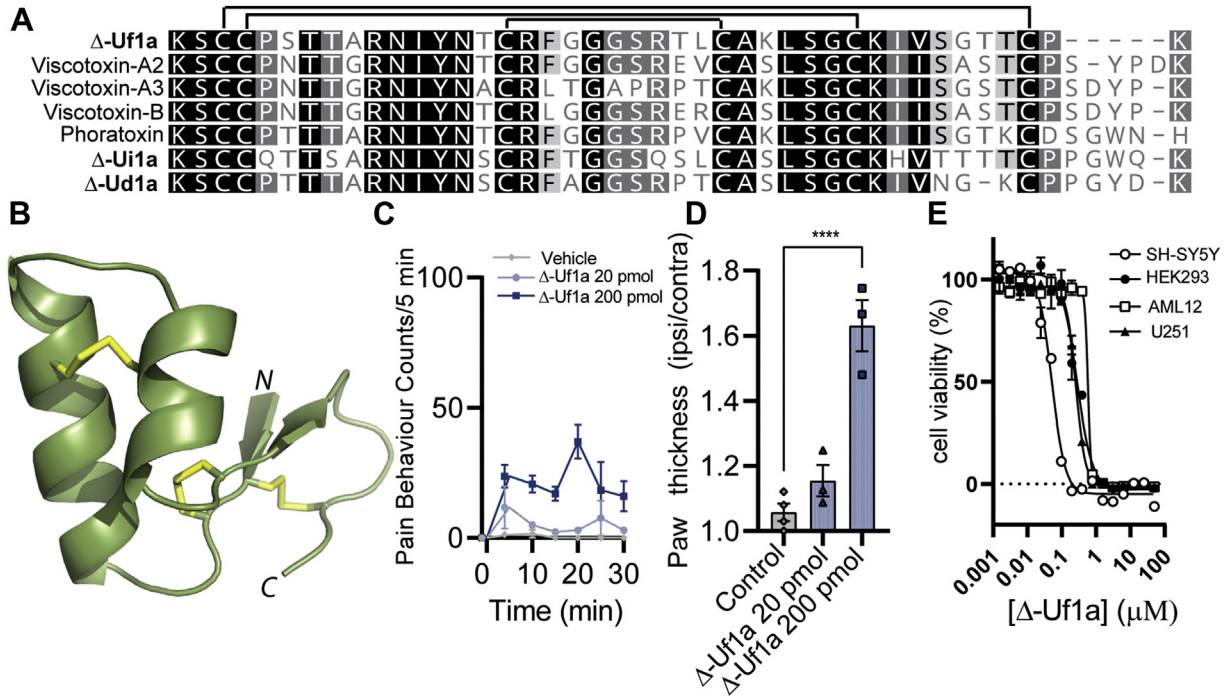

Figure 3. Δ-Uf1a is an algogenic and cytotoxic plant defensin. *A*, alignment of the mature peptide sequences of Δ-Uf1a, viscotoxins (Uniprot P32880, P01538, P08943), phoratoxin (Uniprot P01539), Δ-Ui1a (from an *Urtica incisa* transcriptome, NCBI short read archive [SRA] SRR10567092) and Δ-Ud1a (*Urtica dioica* transcriptome, SRA ERR2040431). *B*, 3D structure of synthetic Δ-Uf1a determined by NMR spectroscopy (PDB ID 7S7P). Disulfide bonds are shown as *yellow sticks*. *C*, spontaneous pain behaviors in mice following shallow intraplantar injection of Δ-Uf1a (20 or 200 pmol). *D*, paw swelling caused by Δ-Uf1a when injected intraplantar into mice. *E*, Δ-Uf1a is a potent cytotoxin. Cell viability was assessed *via* MTT assay after 24 h. Data are expressed as means ± SEM.

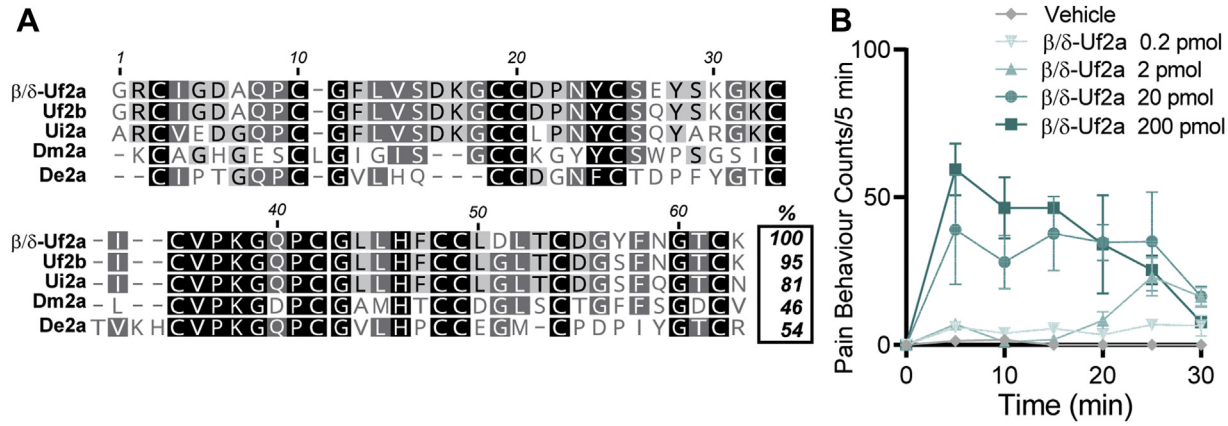

Figure 4. β/δ-Uf2a defines a new class of disulfide-rich plant peptides. *A*, alignment of the mature primary sequences of β/δ-Uf2a and putative paralogues and orthologues identified in transcriptome data and confirmed on cDNA or genomic DNA levels in *U. ferox* (Uf2a and Uf2b), *U. incisa* (Ui2a), *Dendrocnide moroides* (Dm2a) and *D. excelsa* (De2a). Numbering is based on β/δ-Uf2a and % sequence identity relative to β/δ-Uf2a is indicated in the *boxed section*. *B*, spontaneous pain behaviors in mice following shallow intraplantar injection of β/δ-Uf2a (0.2–200 pmol). All data are expressed as means ± SEM.

defense peptides present in various species of mistletoe (14, 15). The theoretical monoisotopic mass (assuming formation of three disulfide bonds from six cysteine residues) of 4364.065 Da was consistent with the experimentally determined monoisotopic mass of subfraction 12.2 (4364.060 Da). In line with recommendations set out for the naming of peptide toxins (16), we named this peptide urthionin-Uf1a (Δ-URTH-Uf1a, or Δ-Uf1a, for short). Δ-Uf1a may be similar or even identical to a crudely purified *U. ferox* molecule described by Dizwani and Laws (12), which had an apparent molecular mass of about 4.2 kDa on gel filtration and was toxic when injected intracerebrally into mice. Additional homologues were identified in the transcriptomes of the Australian nettle *U. incisa* (Ui1a) and the common nettle *U. dioica* (Ud1a, Fig. 3*A*).

The neurotoxic 6.7-kDa component (subfraction 12.6) is a 63-amino-acid peptide with no similarity to any previously described sequence (*i.e.*, no significant matches by TBLASTN against the NCBI nonredundant nucleotide collection). The cysteine scaffold was not related to that of any previously described disulfide-rich peptide families in plants (17, 18), suggesting that this peptide, which we named urticatoxin-Uf2a (β/δ-URTX-Uf2a, β/δ-Uf2a), may adopt a novel, so far uncharacterized, peptide fold. Its predicted monoisotopic mass (6720.803 Da, assuming formation of six disulfide bonds) was consistent with the experimentally determined value for F12.6 (6720.789 Da; Fig. 1*D*).

Δ-*Uf1a is a pain-causing thionin*

For further structural and functional analyses, we used solid phase peptide synthesis (SPPS) to chemically synthesize Δ-Uf1a (Fig. S2). The synthetic material coeluted on RP-HPLC with the principal component in subfraction 12.2, indicating that they are structurally identical (Fig. S2). We determined the three-dimensional structure of synthetic Δ-Uf1a by NMR spectroscopy using NOE distance and angular restraints (Fig. 3*B*, Table S1 and Fig. S3). The NMR data confirmed that Δ-Uf1a adopted a disulfide-stabilized thionin fold, characterized by two antiparallel α-helices in a helix–loop–helix configuration connected to a short antiparallel β-sheet formed by the N and C termini. Like other thionins, Δ-Uf1a contains conserved Lys1 and Tyr13 residues that are important for the cytolytic activity of these molecules (19).

Intraplantar injection of synthetic Δ-Uf1a caused nocifensive responses in mice (Fig. 3*C*) that were indistinguishable from that caused by the native peptide (subfraction 12.2). The minimum effective dose of the toxin (200 pmol or 20 μl intraplantar of a 10 μM solution) caused immediate and long-lasting spontaneous pain behaviors accompanied by swelling and redness of the injected paw (Fig. 3*D*).

β/δ-*Uf2a mediates the systemic toxicity of* U. ferox *sting*

Our attempts to chemically synthesize the larger (6.7-kDa) neurotoxic peptide, β/δ-Uf2a, by SPPS were unsuccessful, and thus our pharmacological analyses were carried out using the purified native peptide (estimated at 98% purity; Fig. S4). The isolated yield for β/δ-Uf2a after two rounds of RP-HPLC was 0.47 mg per 100 mg of lyophilized crude trichome extract.

Intraplantar injection of purified β/δ-Uf2a (0.2–200 pmol) caused dose-dependent, immediate, and long-lasting spontaneous pain behaviors in mice (Fig. 4*B*) that were greater than those caused by the same dose of Δ-Uf1a (Fig. 3*C*), although without any swelling of the injected paw (not shown). The minimum effective dose of β/δ-Uf2a was 0.2 pmol. At the highest dose tested (200 pmol), we observed systemic symptoms including hypokinesia and hypersalivation (n = 3), which began to develop at ∼20 and ∼40 min post injection, respectively. Systemic symptoms, including hypersalivation, have been reported in severe cases of *U. ferox* envenomation in humans and animals (5, 7), and our data suggest that β/δ-Uf2a (and probably other paralogues in the venom) are the responsible agents. One such paralogue is Uf2b that we identified in a *U. ferox* cDNA library and that is highly similar to β/δ-Uf2a (95% sequence identity). We identified additional homologues in the Australian nettle *U. incisa* (Ui2a, 81%) and

the stinging trees *Dendrocnide moroides* (Dm2a, 46%) and *Dendrocnide excelsa* (De2a, 54%) (Fig. 4*A*).

These data indicated that the peptides β/δ-Uf2a and Δ-Uf1a (and probably other paralogues of each) are likely primarily responsible for the painful symptoms of *U. ferox* stings, with β/δ-Uf2a being the more potent of the two toxins.

Δ-Uf1a is a potent cytotoxin

We investigated the mechanism of action of the two toxins. Thionins generally show broad toxicity against a range of organisms and cell lines (19, 20), so we tested the cytotoxic activity of synthetic Δ-Uf1a in a panel of neuronal and nonneuronal cell lines (Fig. 3*E*). Cell viability was quantified *via* MTT assay after 24 h. Δ-Uf1a showed particularly potent cytotoxic activity against the neuroblastoma cell line SH-SY5Y with a half maximal cytotoxic concentration (CC_{50}) of 52 ± 16 nM and slightly weaker activity against the nonneuronal cell lines HEK293 (CC_{50} 278 ± 22 nM), AML12 (CC_{50} 582 ± 22 nM), and U251 (CC_{50} 258 ± 8 nM, all data n = 3). Although the precise mechanism of action of thionins has not been established, there is a general consensus that the broad-spectrum cytotoxic and antimicrobial activity of these toxins involves direct interaction with cell membranes (19, 20). As described above, Δ-Uf1a caused effects in DRG cells indicative of membrane-targeting activity (Fig. 2*B*). Thus, Δ-Uf1a is a cytotoxic and pain-causing peptide whose mechanism of action appears to be *via* the general disruption of cell membranes.

β/δ-Uf2a is an activator of voltage-gated sodium channels

In contrast to Δ-Uf1a, which activated both neuronal and non-neuronal cells, β/δ-Uf2a activated only the neuronal cells in our DRG cultures, and of these, only a subset of the diverse neuronal populations present (Fig. 2, *A* and *C*). This activity was suggestive of a neuron-specific receptor for the peptide. The activation of DRG neurons by β/δ-Uf2a was completely inhibited in the presence of tetrodotoxin (TTX; 1 μM) (Fig. 2*D*), a blocker of a subset of voltage-gated sodium (Na_V) channels, thus implicating TTX-sensitive Na_V channels as the receptor.

Using whole-cell voltage-clamp electrophysiology, we investigated the effects of β/δ-Uf2a on human Na_V channel subtypes $Na_V1.6$, $Na_V1.7$ (both TTX sensitive), and $Na_V1.8$ (TTX resistant), which are among the dominant subtypes in mammalian DRG neurons and have each been implicated in peripheral pain signaling (21), and the human cardiac Na_V channel subtype $Na_V1.5$ (TTX resistant). Representative $Na_V1.5$, $Na_V1.6$, $Na_V1.7$, and $Na_V1.8$ current responses to a step depolarization from −90 to −20 mV (+10 mV for $Na_V1.8$), in the absence and presence of β/δ-Uf2a, are shown in Figure 5, *A*, *D*, *G* and *J*. At $Na_V1.5$, β/δ-Uf2a (1 μM) delayed fast inactivation (τ = 29.8 ± 2.2 ms for β/δ-Uf2a, *versus* 1.13 ± 0.12 ms for control; $p < 0.0001$, paired *t* test, n = 10; Fig. 5*B*) and caused a sustained current ($I_{40\text{-ms}}/I_{peak}$ 44 ± 4% of control; $p < 0.0001$, paired *t* test; n = 10; Fig. 5*B*). Similarly, at $Na_V1.6$, β/δ-Uf2a (300 nM) delayed fast inactivation (τ = 6.14 ± 0.66 ms for β/δ-Uf2a, *versus* 1.23 ± 0.14 ms for control; $p = 0.0073$, paired *t* test, n = 4; Fig. 5*E*) and caused a sustained current ($I_{40\text{-ms}}/I_{peak}$ 41 ± 4% of control; $p = 0.0028$, paired *t* test; n = 4; Fig. 5*E*). At $Na_V1.7$ β/δ-Uf2a (1 μM) delayed fast inactivation (τ = 5.40 ± 0.50 ms for β/δ-Uf2a, *versus* 0.88 ± 0.13 ms for control; $p = 0.0002$, paired *t* test, n = 6; Fig. 5*H*) and caused a small sustained current ($I_{40\text{-ms}}/I_{peak}$ 6.8 ± 1% of control; $p < 0.0034$, paired *t* test; n = 6; Fig. 5*H*). β/δ-Uf2a also caused a hyperpolarizing shift in the voltage dependence of activation of $Na_V1.5$ (ΔV_{50} −6.4 ± 1.6 mV, $p = 0.0145$, paired *t* test; n = 5; 1 μM β/δ-Uf2a, Fig. 5*C*), $Na_V1.6$ (ΔV_{50} −9.0 ± 0.8 mV, $p < 0.0001$, paired *t* test; n = 8; 300 nM β/δ-Uf2a, Fig. 5*F*), and $Na_V1.7$ (ΔV_{50} −11.0 ± 1.5 mV, $p < 0.0001$, paired *t* test; n = 4; 1 μM β/δ-Uf2a, Fig. 5*I*) and a shift in the voltage dependence of steady-state fast inactivation of $Na_V1.6$ (ΔV_{50} −9.3 ± 0.9 mV, $p < 0.0001$, paired *t* test; n = 8, Fig. 5*F*) but not $Na_V1.5$ (ΔV_{50} −3.8 ± 2.8 mV, $p = 0.2387$, paired *t* test; n = 5) or $Na_V1.7$ (ΔV_{50} −1.5 ± 0.6 mV, $p = 0.0817$, paired *t* test; n = 4). Consistent with our *in vitro* DRG data showing complete inhibition of neuronal activation by TTX, β/δ-Uf2a, up to a concentration of 1 μM, did not affect current responses of the TTX-resistant Na_V channel subtype $Na_V1.8$ (Fig. 5*J*). Of the channels tested, $Na_V1.6$ was the most sensitive to β/δ-Uf2a, where the peptide had a half maximal effective concentration (EC_{50}) of 857 ± 127 pM (n = 4; Fig. 5*K*). $Na_V1.5$ had an EC_{50} of 55 ± 1 nM (n = 10; Fig. 5*K*) and $Na_V1.7$ an EC_{50} of 208 ± 52 nM (n = 6; Fig. 5*K*). Collectively, these effects resemble the effects of other gating-modifier toxins (such as α/β-scorpion toxins or δ-conotoxins) and are consistent with enhanced excitability of sensory neurons, and the nocifensive responses observed following intraplantar administration of β/δ-Uf2a in mice, as well as the painful effects experienced in humans following *U. ferox* stings.

Extracellular loops of domain IV are required for β/δ-Uf2a activity on $Na_V1.7$

The extracellular loops of Na_V channels represent discrete binding sites for the majority of the described gating-modifier toxins (22). We exploited the preferential activity of β/δ-Uf2a for $Na_V1.7$ over $Na_V1.8$ to identify the regions of the channel required for the toxin's activity. For these experiments, we used $Na_V1.7$ channel mutants for which the extracellular loops of domain II (DII) S1-S2 DII S3-S4 or domain IV (DIV) S1-S2 and DIV S3-S4 were replaced with the corresponding sequences of $Na_V1.8$ (see Fig. 6*A* for schematic and Table S3). The loop substitutions had no effect on the τ of fast inactivation in the absence of toxin (Fig. S5).

β/δ-Uf2a (1 μM) caused a delay in fast inactivation at wildtype $Na_V1.7$ (τ = 5.0 ± 0.4 ms) that was not significantly decreased when DII S1-S2 (τ = 4.0 ± 0.4 ms; $p = 0.1824$, one-way ANOVA) or DII S3-S4 (τ = 4.3 ± 0.5 ms; $p = 0.3804$, one-way ANOVA) was replaced with $Na_V1.8$ sequences (Fig. 6, *B* and *C*). However, the effect of β/δ-Uf2a on the delay in fast inactivation was significantly decreased when the DIV S1-S2 (τ = 2.7 ± 0.3 ms; $p = 0.0003$, one-way ANOVA) or DIV S3-S4 (τ = 1.6 ± 0.2 ms; $p < 0.0001$, one-way ANOVA) segments were replaced with the corresponding $Na_V1.8$ loops, indicating

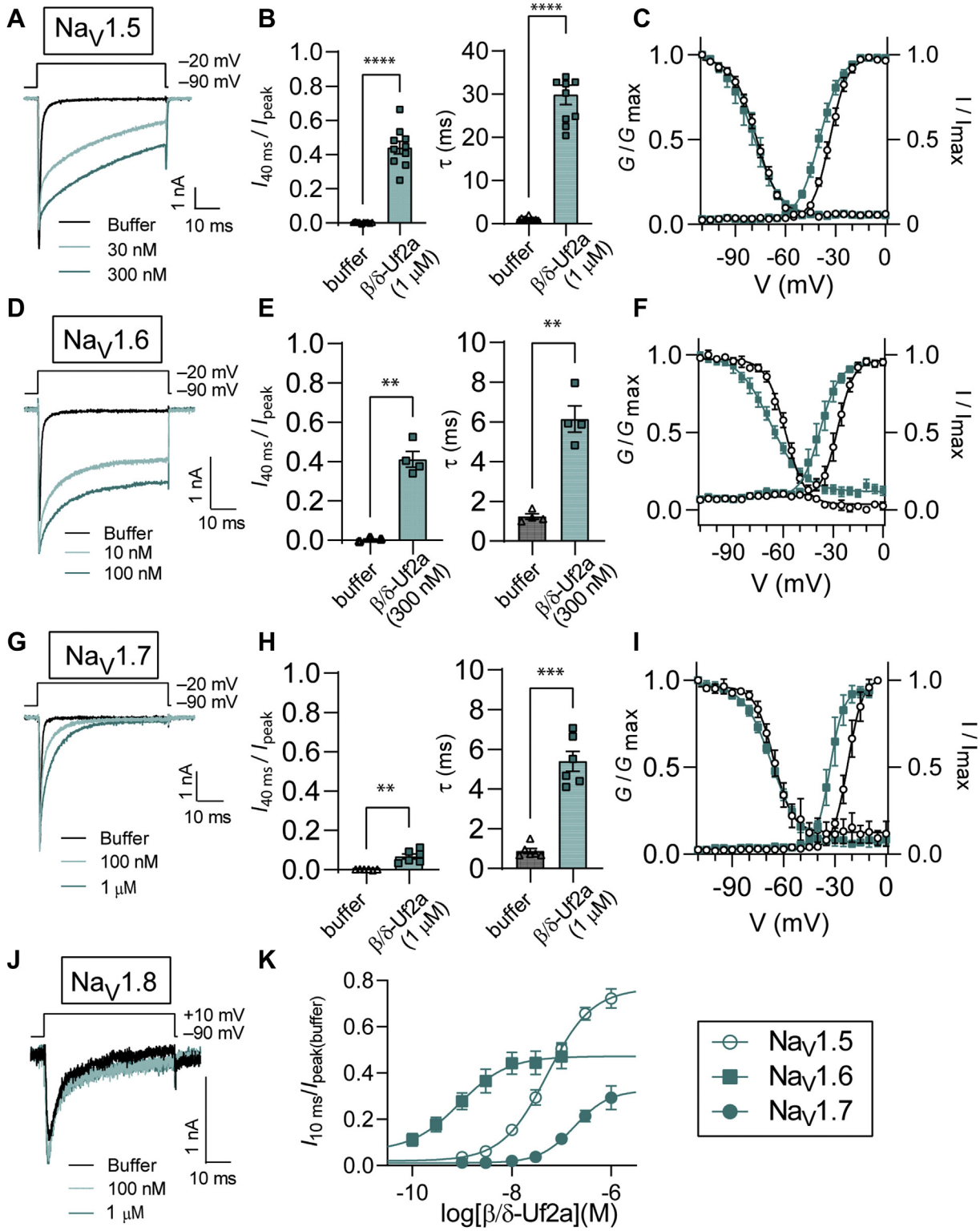

Figure 5. β/δ-Uf2a contributes to the symptoms of *U. ferox* stings *via* modulation of voltage-gated sodium channels. *A*, *D*, *G* and *J*, representative $Na_V1.5$, $Na_V1.6$, $Na_V1.7$, and $Na_V1.8$ current responses to a step depolarization from −90 to −20 mV (+10 mV for $Na_V1.8$) in the absence or presence of β/δ-Uf2a. *B*, *E* and *H*, effects of β/δ-Uf2a on sustained current ($I_{40\ ms}/I_{peak}$) and kinetics of fast inactivation (τ) of $Na_V1.5$ (*B*), $Na_V1.6$ (*E*), and $Na_V1.7$ (*H*), where response is $I_{40\text{-}ms}$ (Current amplitude at 40 ms) after β/δ-Uf2a treatment/peak current (I_{peak}) of cell (before toxin addition). Statistical significance compared with buffer control was determined *via* paired *t* test, $^{**}p < 0.01$, $^{***}p < 0.001$, $^{****}p < 0.0001$. *C*, *F* and *I*, superimposed conductance–voltage (*G–V*) and steady-state fast inactivation curves, before (*open symbols*) and after addition of toxin (*filled symbols*) for $Na_V1.5$ (*C*, 1 μM β/δ-Uf2a), $Na_V1.6$ (*F*, 300 nM β/δ-Uf2a), and $Na_V1.7$ (*C*, 1 μM β/δ-Uf2a). *K*, concentration–response relationship of β/δ-Uf2a modulation of human $Na_V1.5$, $Na_V1.6$, and $Na_V1.7$, where response is $I_{10\text{-}ms}$ (Current amplitude at 10 ms) after β/δ-Uf2a treatment/peak current (I_{peak}) of cell (before toxin addition). All data are expressed as mean ± SEM.

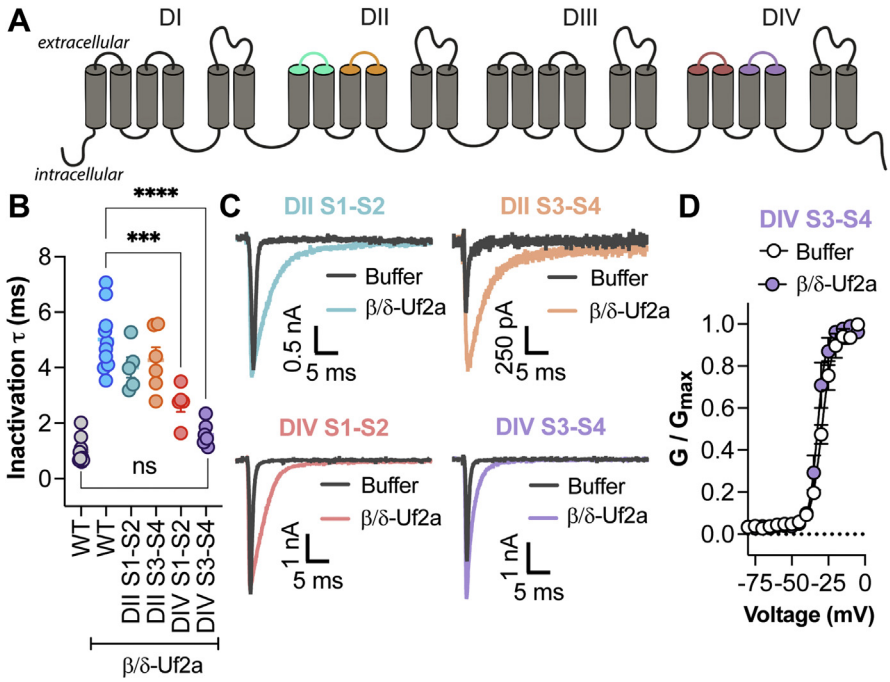

Figure 6. The extracellular loops of domain IV on $Na_V1.7$ mediate the effects of β/δ-Uf2a. *A*, schematic representation of $Na_V1.7$ depicting the extracellular loops on DII and DIV that were replaced with $Na_V1.8$ sequences. *B*, the effect of β/δ-Uf2a (1 μM) on the τ of fast inactivation at $Na_V1.7$ where the DII S1-S2, DII S3-S4, DIV S1-S2, and DIV S3-S4 extracellular loops were replaced by $Na_V1.8$ (n = 5–10). Insertion of $Na_V1.8$ DIV S1-S2 and $Na_V1.8$ DIV S3-S4 loops significantly reduced the activity of β/δ-Uf2a. The loop substitutions had no effect on the τ of fast inactivation in the absence of toxin (Fig. S5). Statistical significance was determined using one-way ANOVA with Dunnett's multiple comparisons test compared with wildtype $Na_V1.7$ with buffer or β/δ-Uf2a as indicated, ***p <0.001, ****p <0.0001. Data are presented as mean ± SEM. *C*, representative current traces from the $Na_V1.7/Na_V1.8$ loop mutant channels before and after addition of β/δ-Uf2a (1 μM). Currents were elicited by a 50-ms pulse to −20 mV (+10 mV for DII S3-S4) from a holding potential of −90 mV. *D*, superimposed conductance–voltage (*G–V*) curves for $Na_V1.7$ where the DIV S3-S4 extracellular loop has been replaced with the corresponding sequence from $Na_V1.8$, before (*white*) and after addition of 1 μM β/δ-Uf2a (*cyan*). $V_{0.5}$: buffer control −29.1 ± 1.1 mV; β/δ-Uf2a −31.9 ± 1.4 mV, p = 0.0539, paired t test, n = 4.

that residues in both the DIV S1-S2 and S3-S4 extracellular loops are required for β/δ-Uf2a modulation of the channel (Fig. 6, *B* and *C*). Numerous venom-derived peptides including α-scorpion toxins, δ-theraphotoxins, and sea anemone toxins, target this binding site, referred to as "site 3," to delay fast inactivation of Na_V channels (22). While our data indicate that site 3 represents a key interaction site for β/δ-Uf2a, additional interactions with residues in neighboring domains are also possible.

Venom-derived peptides that exclusively modulate voltage dependence of channel activation, including β-scorpion toxins and β-theraphotoxins, mediate this effect by binding to the DII S1-S2 and S3-S4 extracellular loops, referred to as "site 4" (22). To preclude the possibility that β/δ-Uf2a is also binding to this site, we next assessed the effect of β/δ-Uf2a on the voltage dependence of activation on the $Na_V1.7/Na_V1.8$ DIV S3-S4 channel mutant. Unlike for wildtype $Na_V1.7$ (see above), β/δ-Uf2a (1 μM) no longer shifted the voltage dependence of activation when DIV S3-S4 was replaced with the corresponding sequence of $Na_V1.8$ (ΔV_{50} −2.8 ± 1.8 mV; p = 0.0539, n = 4, paired t test; Fig. 6*D*), suggesting that the toxin's effects on Na_V channel gating were mediated predominantly through interactions with DIV. Indeed, some site 3 scorpion toxins are reported to both delay fast inactivation and cause a hyperpolarizing shift in the activation threshold, although the latter is often not assessed in toxin-channel mutant studies (23–25).

Distribution of stinging nettle toxins

In a previous study we reported a family of Na_V channel peptide toxins from the venoms of *Dendrocnide* species (also tribe: *Urticeae*) (26). These peptides (gympietides) modulate $Na_V1.7$ by slowing channel inactivation and shifting $V_{1/2}$ of channel activation to a more negative potential. Given the close relationship between the genera *Urtica* and *Dendrocnide* and the related pharmacology of the urticatoxins and gympietides, we investigated whether the urticatoxins and gympietides were homologous, *i.e.*, derived from a common ancestral toxin. Alignment of the precursor sequences of representative members of urticatoxins and gympietides revealed sequence identity of approximately 25% between the two families, whereas identity within each family was substantially higher (75–90%, Fig. S6). This finding suggests that gympietides and urticatoxins are not homologous and is also consistent with the differences in molecular size (4.2 kDa *versus* 6.7 kDa), number of cysteines (six *versus* twelve), cysteine scaffold (cysteine spacing and intercysteine loop size), and likely tertiary structure of the mature peptides.

Next, we explored how widely distributed the three classes of peptide toxins (urthionins, urticatoxins, and gympietides) are among the *Urticeae*, the tribe within the Urticaceae family whose ∼150 members have stinging hairs (4). We analyzed the transcriptomes of *U. ferox*, *U. incisa*, *D. excelsa*, *D. moroides* (NCBI BioProject PRJNA592832), and *U. dioica* (PRJEB21674,

leaves) (26, 27). We also included the assembled *Boehmeria nivea* (1-kP sample ACFP, vegetative tissue) transcriptome as a representative of the Urticaceae that lacks stinging hairs (tribe *Boehmerieae*). We used TBLASTN to search these transcriptomes, using MoTxA, β/δ-Uf2a, and Δ-Uf1a as the query sequences. We detected the recently described gympietides only in transcriptomes of plants of the genus *Dendrocnide*. Δ-Uf1a homologues were detected in transcriptomes of *U. ferox* (n = 5), *U. incisa* (n = 7), and *U. dioica* (n = 9) (Fig. S7); one was detected in *D. excelsa*, whereas none were detected in the transcriptome of *D. moroides*. β/δ-Uf2a homologues were detected in transcriptomes of both *D. excelsa* (n = 6) and *D. moroides* (n = 2), as well as in *U. ferox* (n = 15), *U. dioica* (n = 17), and *U. incisa* (n = 12) (Fig. S8). No homologous peptides sharing >40% identity were detected in the transcriptome of *B. nivea*, suggesting none of these peptide families are expressed in *B. nivea*. Although further work will be needed to demonstrate that the homologues identified in the above transcriptomes are indeed toxins (rather than nontoxic peptides or pseudogenes), our analysis of the distribution of the three pain-inducing toxin families in Urticaceae suggests that (i) their expression is restricted to the stinging trichome-producing lineage (tribe *Urticeae*), (ii) the urthionin and urticatoxin families are found in both *Urtica* and *Dendrocnide* and thus were present in their common ancestor, and that (iii) the gympietides are a unique innovation of the genus *Dendrocnide*.

Discussion

The pharmacology of nettle stings has attracted attention for centuries, with the nature and identity of pharmacologically active substances being the subject of intense debate (3, 28–30). Small molecule neurotransmitters or inflammatory mediators such as acetylcholine, histamine, or serotonin have been identified in the trichomes of several species from the Urticaceae family (4), but this study adds to the accumulating evidence that at least some of the major pharmacological effects of nettle stings are caused by disulfide-rich peptides. For example, we recently identified inhibitory cystine knot peptides (gympietides) as the principal pain-causing agents in the stinging hairs of the Australasian stinging trees (genus *Dendrocnide*) (26). Here we report the identification of two different disulfide-rich peptide families as the principal agents mediating the effects of *U. ferox* sting: a thionin (Δ-Uf1a) and a neurotoxin (β/δ-Uf2a) that defines a previously unrecognized class of disulfide-rich peptides. While the mechanism of action of the cytolytic Δ-Uf1a is consistent with disruption of membrane integrity, the activity of the neurotoxic β/δ-Uf2a resembles the effects of animal toxins targeting site 3 on Na_V channels, for example, scorpion α-toxins and δ-conotoxins (22). However, β/δ-Uf2a does not share any sequence similarity with these animal toxins (or any other known Na_V-modulatory peptides) revealing the convergent evolution of Na_V site 3–targeting toxins in the animal and plant kingdoms. These observations also demonstrate that members of Urticaceae have recruited multiple classes of peptide toxins that increase neuronal excitability.

β/δ-Uf2a was active at $Na_V1.5$, $Na_V1.6$, and $Na_V1.7$ but inactive (at 1 μM) at $Na_V1.8$. This difference in activity may be due to the three-amino-acid residue extension in the DIV S3-S4 loop of $Na_V1.8$ that is not present in $Na_V1.1$ to 1.7 (Table S4). Given that the DIV S3-S4 loop is highly conserved at $Na_V1.1$ to 1.7, it is thus likely that β/δ-Uf2a is also active at $Na_V1.1$ to 1.4, although this remains to be experimentally confirmed. However, binding to the DIV S3-S4 loop alone does not explain the >200-fold potency difference of β/δ-Uf2a between $Na_V1.6$ and $Na_V1.7$. Therefore, it is likely that residues in the DIV S1-S2 loop, which is less conserved between $Na_V1.1$ to 1.7, also form important interactions with β/δ-Uf2a, which is consistent with our $Na_V1.7$/$Na_V1.8$ S1-S2 loop substitution data.

Interestingly, a common molecular mechanism underlying the painful effects of stinging nettles is emerging, with both the gympietides and urticatoxins having evolved to modulate vertebrate Na_V channels. While the precise mechanisms of action and binding sites of these peptide families remains to be established, both the gympietides and urticatoxins inhibit inactivation of voltage-gated sodium channels, rendering neurons hyperexcitable. Given that the gympietides and urticatoxins vary in their size, number of disulfides, and spacing between disulfides, we propose that these families are probably not homologous and were recruited to venom separately, thus representing an example of convergence. The reason underlying the emergence of a distinct class of pain-causing Na_V channel toxin in *Dendrocnide*, when urticatoxins were presumably already present, is interesting to consider. Did *Dendrocnide* encounter a predator, not faced by *Urtica*, which was resistant or developed resistance to the urticatoxins and drove the recruitment of a new class of defensive toxin, the gympietides? Further investigation of the history of these nettle toxin families and the ecology of different Urticaceae is warranted.

It is generally accepted that the stings of many *Urtica* species are an effective deterrent against browsing/grazing from large mammalian herbivores (4). In this context, it is interesting to consider that *U. ferox* was present in New Zealand for tens of millions of years in the absence of any large mammalian herbivores, yet retained its powerful defensive sting. Until ∼500 years ago, the ecological niche filled by large mammalian herbivores on other land masses was occupied in New Zealand by several species of large flightless bird known as the moa (order: *Dinornithiformes*). Larger moa grew to >3 m in height and weighed >200 kg. One can speculate that, in New Zealand, grazing by these birds may have been a major driving force behind the toxicity of *U. ferox* stings. Indeed, recent investigations of subfossil moa gizzard contents and coprolites have shown that *Urtica* was part of the diet of several moa species (31).

In summary, our findings suggest that urthionin and urticatoxin peptides are the principal pain-causing agents mediating the effects of *U. ferox* stings and suggest that the latter may also play a role in the reported systemic effects. Our data suggest that homologues of these toxins are likely to be the pain-causing agents underlying the stings of other *Urticeae*, including the common nettle (*U. dioica*). Stinging trichomes

are not an exclusive innovation of the Urticaceae and can also be found in other plant families, most notably Loasaceae and Euphorbiaceae, which together have been estimated to have around 450 stinging representatives (4). While it is too early to speculate on the nature of these non-*Urticaceae* stinging toxins, our data highlight stinging plants as a potentially rich, but so far underexplored, source of novel neuroactive peptides.

Experimental procedures

Plant cultivation and peptide extraction and purification

Seeds of *U. ferox* were obtained from New Zealand Tree Seeds and grown in Jiffy peat pots. Trichomes were cut from leaves and stems with a scissor and were ground in liquid nitrogen then lyophilized on a freeze drier (CHRIST Alpha 2-4 LD). The dried trichomes (883 mg) were crushed to a fine powder in a bead mill (Geno/Grinder, 1200 rpm for 3 min), then extracted using 50% acetonitrile (ACN) in 1% formic acid solution (1 ml solution per 20 mg dried trichome tissue) at room temperature. After overnight extraction, the solution was cleared by centrifugation at 3900*g* for 30 min, filtered through a 0.45-µm filter, then lyophilized on the freeze drier (yield: 336 mg of crude extract).

Freeze-dried crude extracts (110 mg) were dissolved in 5% ACN 0.05% TFA, then purified by RP-HPLC (buffer A: 0.05% trifluoroacetic acid [TFA] in H_2O; buffer B: 90% ACN with 0.05% TFA) using a Phenomenex C18 column (250 × 10 mm) with a gradient of 5 to 80% buffer B in buffer A over 40 min. Active fractions were further purified by RP-HPLC with a Luna C18 (250 × 4.6 mm) column using a linear gradient of 20 to 50% buffer B in buffer A over 90 min.

Chemical synthesis of Δ-Uf1a

Δ-Uf1a was chemically synthesized by automated Fmoc SPPS using optimized protocols. The peptide was assembled on 2-chlorotrityl chloride resin using the following side chain–protecting groups: Cys(Trt), Lys(Boc), Asn(Trt), Arg(Pbf), Ser(tBu), Thr(tBu), and Tyr(tBu). After assembly, resin cleavage and side-chain deprotection were carried out by suspending the dried peptide-resin in cleavage cocktail (TFA:triisopropylsilane:H2O; 95:2.5:2.5). After stirring for 1 h at room temperature, TFA was evaporated and the peptide was precipitated with cold diethyl ether. The peptide was dissolved in 50% ACN/water containing 0.05%TFA and lyophilized. Crude peptides were dissolved in a 10% (v/v) ACN–water mixture containing 0.05% (v/v) TFA, before being purified by preparative HPLC. The column was equilibrated with 10% of solvent B (ACN:H_2O:TFA; 89.95:10:0.05) in solvent A (H_2O:TFA; 99.95:0.05). Peptides were eluted using linear gradients of solvent B in solvent A, and fractions were collected across the expected elution time. Peptide purity and identity were assessed by electrospray ionization mass spectrometry (ESI-MS) on Shimadzu 2020 LC mass spectrometer and by analytical scale HPLC on a Shimadzu Nexera system equipped with an Agilent Zorbax C18 column (1.8 mm, 2.1 × 100 mm). Fractions containing the desired product were pooled, lyophilized, and stored at −20 °C. Observed masses: m/z 875.3 $[M+5H]^{5+}$, m/z 1093.9 $[M+4H]^{4+}$, and m/z 1458.2 $[M+3H]^{3+}$ (ESI-MS); calculated masses (average isotope composition): m/z 875.4 $[M+5H]^{5+}$, m/z 1094.0 $[M+4H]^{4+}$, and m/z 1458.3 $[M+3H]^{3+}$.

Folding and disulfide formation were carried out by incubating the purified reduced peptide in folding buffer (200 mM ammonium bicarbonate, 5 mM reduced glutathione, 0.5 mM oxidized glutathione, pH 8.5) at a peptide concentration of 0.2 mg/ml. After stirring at 23 °C for 4 h the principal product was isolated by preparative HPLC as described above. Observed masses: m/z 874.2 $[M+5H]^{5+}$, m/z 1092.4 $[M+4H]^{4+}$, and m/z 1456.4 $[M+3H]^{3+}$ (ESI-MS); calculated masses (average isotope composition): m/z 874.2 $[M+5H]^{5+}$, m/z 1092.5 $[M+4H]^{4+}$, and m/z 1456.4 $[M+3H]^{3+}$.

Nuclear magnetic resonance spectroscopy and structure calculations

NMR spectroscopy was performed on Bruker Avance III HD 600 MHz equipped with a cryogenically cooled probe. Samples of synthetic Δ-Uf1a (2.2 mg) were prepared in 500 µl of 10% (v/v) D_2O in water, pH 4.1. Two dimensional experiments including TOCSY (80 ms mixing time), NOESY (200 ms mixing time), exclusive COSY, and natural abundance ^{15}N and ^{13}C-heteronuclear single quantum coherence were used to sequentially assign backbone and side-chain protons and heteroatoms. Variable temperature experiments were performed by recording six TOCSY spectra at temperatures ranging from 283 to 308 K. Slowly exchanging amide protons were identified by dissolving lyophilized Δ-Uf1a in 100% D_2O and monitoring H/D exchange over 24 h. Solvent suppression was achieved using excitation sculpting. Spectra were referenced to water at 4.77 ppm. All spectra were processed using Topspin v3.6 and assigned using CcpNMR Analysis v2.4.2.

Distance restraints derived from the NOESY spectrum were used to calculate preliminary structures of Δ-Uf1a in CYANA (32), along with dihedral angles predicted by TALOS-N (33). Hydrogen bond pairs were added based upon these preliminary structures, amide proton temperature dependence, and slow deuterium exchange of proton donors. A final ensemble of structures was generated within the program CNS (34) using torsion angle dynamics and refinement and energy minimization in explicit water solvent. Stereochemical quality was assessed using MolProbity (35). Statistics describing the structural analyses are summarized in Table S1.

mRNA isolation and transcriptome analysis

U. ferox samples (leaves and shoots) were collected near Mahoenui, New Zealand and immediately preserved in RNAlater (Invitrogen). Total RNA was extracted from preserved *U. ferox* leaves using a NucleoSpin RNA Plant extraction kit (MACHEREY-NAGEL) using the RAP lysis buffer provided, according to the manufacturer's instructions. The resultant RNA was then treated with DNase also provided in this kit. The sample was sequenced on an Illumina HiSeq2500 (Illumina Inc) at the Australian Genome Research Facility (AGRF, Melbourne, Australia) using the NovaSeq pipeline for

100 bp paired-end reads. Data were then assembled using Trinity v2.10.0 (36) after trimming and filtering adapter sequences and poor-quality bases using Trimmomatic v0.38 (37). The assembled transcripts were translated into six reading frames to create a peptide database for MSMS identification. Transcript databases cited in this work were searched using TBLASTN (38) and query peptide sequences. Transcript hits were annotated manually using Geneious v6 (Biomatters Ltd).

Cloning

Genomic DNA (gDNA) was extracted using plant DNA preparation kit (Jena Bioscience). Coding sequences of interest peptides were amplified from cDNA/gDNA by high-fidelity polymerase chain reactions (PCRs) using Phusion polymerase cycled with the following conditions: 30 s of initial denaturation at 98 °C followed by five cycles of 98 °C for 10 s, 57 °C for 20 s, 72 °C for 30 s, and 30 cycles of 98 °C for 10 s and 72 °C for 30 s, with a final extension step of 72 °C for 2 min. Primers were designed at the start and stop of putative transcripts obtained in the assembled transcriptomes and listed in Table S2. Amplified gene products were purified from agarose gels and cloned into the vector pDS221 using BP Clonase (Invitrogen). Purified plasmids were Sanger sequenced by the AGRF.

Tandem MS

Lyophilized peptide sample was dissolved in 0.1 M of NH_4HCO_3, pH 7.8 before reduction with 10 mM dithiothreitol at 60 °C for 30 min. The reduced sample was S-alkylated through the addition of iodoacetamide with the final concentration of 25 mM, then incubated at room temperature at dark for 30 min. Reduced and alkylated sample was then digested with trypsin at 37 °C for 20 h. The reaction was quenched by adding 10% formic acid to a final concentration of 1% formic acid, then analyzed by a Shimadzu UPLC interfaced with an AB Sciex 5600 TripleTOF MS using information dependent acquisition scanning. MS experiment was conducted on an Agilent Zorbax C18 UPLC 300-Å column (100 × 2.1 mm, 1.8 μm) with a linear gradient of 1 to 70% acetonitrile in 49 min. All data were processed using Analyst software by AB Sciex.

MALDI MS

Matrix-assisted laser desorption ionization (MALDI) mass spectrometry was carried out using a TIMS TOF Flex MALDI-2 (Bruker) operated in TIMS off (or QqTOF only) mode, controlled using TIMS Control 1.1.19.68. Positive mode analyses were undertaken over *m/z* 1000 to 10,000, 4000 shots with laser repetition rate of 10,000 Hz, Funnel 1 RF 500 Vpp, Funnel 2 RF 400 Vpp, Multiple RF 600 Vpp, isCID 70 eV, Deflection Delta 70 V, MALDI plate offset 30 V, transfer time of 150 μs, prepulse storage of 20 μs, Collision RF 4000, and collision energy of 10 eV. Calibration was performed using a single spot of α-Cyano-4-hydroxycinnamic acid with Bruker peptide and protein calibration mixtures. Data were visualized using Data Analysis 5.3.

Cell cytotoxicity assay

All mammalian cells were maintained at 37 °C in a humidified atmosphere containing 5% CO_2 and passaged at 80% confluence. Human embryonic kidney (HEK293), glioblastoma (U-251), and mouse hepatocyte (AML12) cell lines were cultured in Dulbecco's modified Eagle's medium (Gibco) supplemented with 10% fetal bovine serum (FBS)/1% penicillin–streptomycin. Human neuroblastoma (SH-SY5Y) was cultured in RPMI 1640 medium (Gibco) supplemented with 15% FBS/1% penicillin–streptomycin/2 mM L-glutamine. Passages between 2 and 10 were used for all cell lines; 5×10^3 cells/well were used for all cells in a 96-well plate. All cells were allowed to attach for 24 h after plating. Media were replaced with serum-free media for cell cytotoxicity assays on the following day. Δ-Uf1a was tested with cells for 24 h at varying final peptide concentrations (0.006 nM–50 μM) in triplicate. MTT (10 μl; 5 mg ml^{-1} in PBS) was added at the end of peptide incubation with cells. The supernatant was then removed followed by the addition of 100 μl dimethyl sulfoxide to solubilize formazan salts. Cell numbers were followed at 600 nm on a Tecan Infinite M1000Pro plate reader.

Pain behavior experiments

Male 5- to 6-week-old C57BL/6J mice used for behavioral experiments were purchased from the Animal Resources Centre (WA, Australia). They were housed in groups of up to four per cage, maintained on a 12/12 h light–dark cycle, and fed standard rodent chow and water *ad libitum*. Fractions, subfractions, or purified/synthetic peptides diluted in saline containing 0.1% bovine serum albumin (BSA) were administered in a volume of 20 μl into the hind paw by shallow intraplantar injection. Negative control animals were injected with saline containing 0.1% BSA. Following injection, spontaneous pain behavior events were counted from video recordings, by a blinded experimenter. Experiments involving animals were approved by The University of Queensland Animal Ethics Committee (approval number 2021/AE000448).

Calcium imaging assay of mammalian sensory neurons

DRG cells were isolated from 4- to 6-week-old male C57BL/6 mice that were purchased from the Animal Resources Centre. DRGs were dissociated, then cells were plated in Dulbecco's Modified Eagle's Medium (Gibco) containing 10% FBS (Assaymatrix) and penicillin/streptomycin (Gibco) on a 96-well poly-D-lysine-coated culture plate (Corning) and maintained overnight. Cells were loaded with Fluo-4 AM calcium indicator, according to the manufacturer's instructions (ThermoFisher Scientific). After loading (1 h), the dye-containing solution was replaced with assay solution (1× Hanks' balanced salt solution, 20 mM Hepes). Images were acquired at 10× objective at 1 frame/s (excitation 485 nm, emission 521 nm). Fluorescence corresponding to $[Ca^{2+}]_i$ of ∼200 cells per experiment was monitored in parallel using an Nikon Ti-E Deconvolution inverted microscope, equipped with a Lumencor Spectra LED Lightsource. Baseline fluorescence was monitored for 30 s. At 30 s, the assay solution was

replaced with either assay solution or assay solution containing TTX (1 μM), then at 1 min with test peptide (in assay solution ± TTX) and monitored for 2 min before being replaced with assay solution and then KCl (30 mM; positive control). Experiments involving the use of mouse tissue were approved by the University of Queensland Animal Ethics Committee (UQ AEC; approval number TRI/IMB/093/17).

Whole-cell voltage-clamp electrophysiology

HEK293 cells stably transfected with human $Na_V1.5/\beta1$, $Na_V1.6/\beta1$, $Na_V1.7/\beta1$, or $\beta1//\beta2$ alone used for transient transfections (SB Drug Discovery) and CHO cells stably transfected with human $Na_V1.8/\beta3$ in a tetracycline-inducible system (ChanTest) were cultured with MEM supplemented with 10% FBS, 2 mM L-glutamine, and selection antibiotics as recommended by the manufacturer.

$Na_V1.7$ mutants were transiently transfected using Lipofectamine 2000 (Thermo Fisher Scientific) and used for patch-clamp experiments 48 h after transfection. The WT $hNa_V1.7$ cDNA (NM_002977, a kind gift from Dr James Cox, University College London) was subjected to *in vitro* site-directed mutagenesis using the QuikChange XL mutagenesis kit (Agilent Technologies) following the manufacturer's instructions. $Na_V1.7$ mutants were generated by replacing the extracellular S1-S2 and S3-S4 loops of domain II (DII) and domain IV (DIV) with the corresponding loop sequences of $Na_V1.8$. Sequences were verified by the AGRF.

Whole-cell patch-clamp experiments were performed on a QPatch-16 automated electrophysiology platform (Sophion Bioscience). The extracellular solution (ECS) contained 145 mM NaCl (replaced with 70 Choline Chloride for $Na_V1.5$ [I-V experiments] $Na_V1.7$ [all experiments]), 4 mM KCl, 2 mM $CaCl_2$, 1 mM $MgCl_2$, 10 mM Hepes, and 10 mM glucose (pH 7.4; osmolarity, 305 mOsm). The intracellular solution contained 140 mM CsF, 1 mM/5 mM EGTA/CsOH, 10 mM Hepes, and 10 mM NaCl (pH 7.3) with CsOH (osmolarity, 320 mOsm). Peptides were diluted in ECS with 0.1% BSA. TTX (1 μM) was added to the ECS for $Na_V1.8$ recordings to inhibit background endogenous TTX-sensitive current in CHO cells. Whole-cell currents were filtered at 8 kHz and acquired at 25 kHz, and the linear leak was corrected by P/4 subtraction. Conductance–voltage (*G–V*) and steady state fast inactivation protocols were recorded with 70% fast series resistance compensation.

Concentration–response experiments were performed using a holding potential of −90 mV and a 50-ms pulse to −20 mV (+10 mV for $Na_V1.8$) every 20 s (0.05 Hz). The time constant of fast inactivation (τ) was computed by fitting the current decay traces with a single exponential function using the QPatch Assay Software 5.6 (Sophion). *I–V* curves were obtained with a holding potential of −90 mV followed by a series of 500-ms step pulses that ranged from −110 to +55 mV in 5-mV increments (repetition interval, 5 s) before and after 5-min incubation with β/δ-Uf2a. Conductance–voltage curves were obtained by calculating the conductance (G) at each voltage (V) using the equation $G = I/(V - V_{rev})$, where V_{rev} is the reversal potential, and were fitted with a Boltzmann equation. Voltage dependence of steady-state fast inactivation was tested using a 10-ms pulse of −20 mV immediately after the 500-ms step above to assess the available noninactivated channels. Inactivation curves were obtained by fitting the data with a Boltzmann equation. For statistical comparison of *G–V* and steady state fast inactivation curves, a two-tailed paired *t* test was used.

Statistics

All data were plotted and analyzed using GraphPad Prism (v9.1.0). Data were fitted to equations as indicated. Statistical significance was defined as $p < 0.05$ using tests as indicated. All data are presented as means ± SEM.

Data availability

RNA sequencing data were deposited in the NCBI Short Read Archive under BioProject accession number PRJNA592832. Nucleotide sequences coding for peptides identified in this study were deposited in NCBI GenBank: Δ-URTH-Uf1a (OK376605), β/δ-URTX-Uf2a (OK376600), URTX-Uf2b (OK376601), URTX-Ui2a (OK376602), URTX-Dm2a (OK376603), and URTX-De2a (OK376604). The structure of Δ-URTH-Uf1a was deposited in RCSB Protein Data Bank (PDB ID: 7S7P) and chemical shift data in Biological Magnetic Resonance Data Bank (BMRB entry: 30951).

Supporting information—This article contains supporting information.

Acknowledgments—We acknowledge the facilities and the scientific and technical assistance of Microscopy Australia and the Centre for Microscopy and Microanalysis, The University of Queensland. Danny Robinson and Cristopher Barker assisted with plant sample collection.

Author contributions—S. D. R., E. K. G., I. V., and T. D. conceptualization; J. X., S. D. R., E. K. G., F. B. H. R., I. V., and T. D. methodology; J. X., S. D. R., E. K. G., S. J., J. R. D., F. B. H. R., K. Y., L. R., L. Y. C., B. R. H., P. J. H., I. V., T. D., and D. J. C. formal analysis; J. X., S. D. R., E. K. G., S. J., J. R. D., F. B. H. R., K. Y., L. R., L. Y. C., B. R. H., P. J. H., I. V., and T. D. investigation; L. R. and D. J. C. resources; J. X., S. D. R., E. K. G., J. R. D., I. V., and T. D. writing – original draft; I. V. and T. D. writing – review & editing; I. V. and T. D. supervision; I. V. and T. D. project administration; D. J. C., I. V., and T. D. funding acquisition.

Funding and additional information—This work was funded by Australian Research Council (ARC) discovery project DP200102377 (I. V. and T. D.), an ARC Laureate fellowship FL150100146 (D. J. C.) and Centre of Excellence (CE200100012) and NHMRC fellowships APP1162503 (I. V.) and APP1139961 (J. R. D.).

Conflict of interest—The authors declare that they have no conflicts of interest with the contents of this article.

Abbreviations—The abbreviations used are: ACN, acetonitrile; AGRF, Australian Genome Research Facility; BSA, bovine serum albumin; DRG, dorsal root ganglion; ECS, extracellular solution; ESI-MS, electrospray ionization mass spectrometry; FBS, fetal

bovine serum; MS, mass spectrometry; MSMS, tandem mass spectrometry; NaV, voltage-gated sodium; RP-HPLC, reversed-phase HPLC; SPPS, solid phase peptide synthesis; TTX, tetrodotoxin.

References

1. Parthasarathy, A., Borrego, E. J., Savka, M. A., Dobson, R. C. J., and Hudson, A. O. (2021) Amino acid-derived defense metabolites from plants: a potential source to facilitate novel antimicrobial development. *J. Biol. Chem.* **296**, 100438
2. War, A. R., Paulraj, M. G., Ahmad, T., Buhroo, A. A., Hussain, B., Ignacimuthu, S., *et al.* (2012) Mechanisms of plant defense against insect herbivores. *Plant Signal. Behav.* **7**, 1306–1320
3. Pilgrim, R. L. C. (1959) Some properties of the sting of the New-Zealand nettle, Urtica-ferox. *Proc. R. Soc. B* **151**, 48–56
4. Ensikat, H. J., Wessely, H., Engeser, M., and Weigend, M. (2021) Distribution, ecology, chemistry and toxicology of plant stinging hairs. *Toxins* **13**, 141
5. Kittow, N. C. (2013) A case of canine poisoning with New Zealand Tree Nettle (Ongaonga, Urtica ferox). *N. Z. Vet. J.* **61**, 60–62
6. Hammond-Tooke, G. D., Taylor, P., Punchihewa, S., and Beasley, M. (2007) Urtica ferox neuropathy. *Muscle Nerve* **35**, 804–807
7. Clark, F. P. (1993) Tree nettle (Urtica-ferox) poisoning. *N. Z. Med. J.* **106**, 234
8. Connor, H. E. (1977). In: Connor, H. E., Keating, E. C., eds. *The Poisonous Plants in New Zealand*, Government Printer, Wellington, NZ: 182–184
9. Blackman, J. G., and Sumich, M. (1966) Pharmacologically active substances in the sting of the New Zealand Nettle Urtica ferox. *Proc. Univ. Otago Med. Sch.* **44**, 25–27
10. Parry, G. J., and Buenz, E. J. (2018) Adventures in self experimentation. *Br. Med. J.* **363**, k5006
11. Kanzaki, M., Tsuchihara, T., McMorran, D., Taylor, P., and Hammond-Tooke, G. D. (2010) A rat model of Urtica ferox neuropathy. *Neurotoxicology* **31**, 709–714
12. Dizwani, A. G. M., and Laws, G. F. (1981) Toxins of the New-Zealand nettle Urtica-ferox. *Proc. Univ. Otago Med. Sch.* **59**, 70–72
13. Willox, S. (1969) *An Investigation of the New Zealand Stinging Nettle Urtica Ferox*. Thesis (M. Pharm), University of Otago
14. Johansson, S., Gullbo, J., Lindholm, P., Ek, B., Thunberg, E., Samuelsson, G., *et al.* (2003) Small, novel proteins from the mistletoe Phoradendron tomentosum exhibit highly, selective cytotoxicity to human breast cancer cells. *Cell. Mol. Life Sci.* **60**, 165–175
15. Jung, M. L., Baudino, S., Ribereaugayon, G., and Beck, J. P. (1990) Characterization of cytotoxic proteins from mistletoe (Viscum-album L). *Cancer Lett.* **51**, 103–108
16. King, G. F., Gentz, M. C., Escoubas, P., and Nicholson, G. M. (2008) A rational nomenclature for naming peptide toxins from spiders and other venomous animals. *Toxicon* **52**, 264–276
17. Silverstein, K. A. T., Moskal, W. A., Wu, H. C., Underwood, B. A., Graham, M. A., Town, C. D., *et al.* (2007) Small cysteine-rich peptides resembling antimicrobial peptides have been under-predicted in plants. *Plant J.* **51**, 262–280
18. Tam, J. P., Wang, S. J., Wong, K. H., and Tan, W. L. (2015) Antimicrobial peptides from plants. *Pharmaceuticals* **8**, 711–757
19. Stec, B. (2006) Plant thionins - the structural perspective. *Cell. Mol. Life Sci.* **63**, 1370–1385
20. Florack, D. E. A., and Stiekema, W. J. (1994) Thionins - properties, possible biological roles and mechanisms of action. *Plant Mol. Biol.* **26**, 25–37
21. Bennett, D. L., Clark, A. J., Huang, J. Y., Waxman, S. G., and Dib-Hajj, S. D. (2019) The role of voltage-gated sodium channels in pain signaling. *Physiol. Rev.* **99**, 1079–1151
22. Deuis, J. R., Mueller, A., Israel, M. R., and Vetter, I. (2017) The pharmacology of voltage-gated sodium channel activators. *Neuropharmacology* **127**, 87–108
23. Huang, Y., Zhou, X., Tang, C., Zhang, Y. X., Tao, H., Chen, P., *et al.* (2015) Molecular basis of the inhibition of the fast inactivation of voltage-gated sodium channel Nav1.5 by tarantula toxin Jingzhaotoxin-II. *Peptides* **68**, 175–182
24. Chen, H., and Heinemann, S. H. (2001) Interaction of scorpion alpha-toxins with cardiac sodium channels: binding properties and enhancement of slow inactivation. *J. Gen. Physiol.* **117**, 505–518
25. Durek, T., Vetter, I., Wang, C. I. A., Motin, L., Knapp, O., Adams, D. J., *et al.* (2013) Chemical engineering and structural and pharmacological characterization of the alpha-scorpion toxin OD1. *ACS Chem. Biol.* **8**, 1215–1222
26. Gilding, E. K., Jami, S., Deuis, J. R., Israel, M. R., Harvey, P. J., Poth, A. G., *et al.* (2020) Neurotoxic peptides from the venom of the giant Australian stinging tree. *Sci. Adv.* **6**, eabb8828
27. Leebens-Mack, J. H., Barker, M. S., Carpenter, E. J., Deyholos, M. K., Gitzendanner, M. A., Graham, S. W., *et al.* (2019) One thousand plant transcriptomes and the phylogenomics of green plants. *Nature* **574**, 679–685
28. Haberlandt, G. (1886) Zur Anatomie und Physiologie der pflanzlichen Brennhaare. *Sitz.-Ber. Akad. Wien.* **93**, 123–145
29. Emmelin, N., and Feldberg, W. (1947) The mechanism of the sting of the common nettle (Urtica-Urens). *J. Physiol.* **106**, 440–455
30. Thurston, E. L., and Lersten, N. R. (1969) The morphology and toxicology of plant stinging hairs. *Bot. Rev.* **35**, 393–412
31. Wood, J. R., Richardson, S. J., McGlone, M. S., and Wilmshurst, J. M. (2020) The diets of moa (Aves: Dinornithiformes). *N. Z. J. Ecol.* **44**, 3397
32. Guntert, P., and Buchner, L. (2015) Combined automated NOE assignment and structure calculation with CYANA. *J. Biomol. NMR* **62**, 453–471
33. Shen, Y., and Bax, A. (2013) Protein backbone and sidechain torsion angles predicted from NMR chemical shifts using artificial neural networks. *J. Biomol. NMR* **56**, 227–241
34. Brunger, A. T., Adams, P. D., Clore, G. M., DeLano, W. L., Gros, P., Grosse-Kunstleve, R. W., *et al.* (1998) Crystallography & NMR system: a new software suite for macromolecular structure determination. *Acta Crystallogr. D* **54**, 905–921
35. Chen, V. B., Arendall, W. B., Headd, J. J., Keedy, D. A., Immormino, R. M., Kapral, G. J., *et al.* (2010) MolProbity: all-atom structure validation for macromolecular crystallography. *Acta Crystallogr. D* **66**, 12–21
36. Grabherr, M. G., Haas, B. J., Yassour, M., Levin, J. Z., Thompson, D. A., Amit, I., *et al.* (2011) Full-length transcriptome assembly from RNA-Seq data without a reference genome. *Nat. Biotechnol.* **29**, 644–652
37. Bolger, A. M., Lohse, M., and Usadel, B. (2014) Trimmomatic: a flexible trimmer for Illumina sequence data. *Bioinformatics* **30**, 2114–2120
38. Altschul, S. F., Gish, W., Miller, W., Myers, E. W., and Lipman, D. J. (1990) Basic local alignment search tool. *J. Mol. Biol.* **215**, 403–410